ACS APPLIED MATERIALS & INTERFACES

Research Article

www.acsami.org

Clear Antismudge Unimolecular Coatings of Diblock Copolymers on Glass Plates

Danielle Macoretta,[†] Muhammad Rabnawaz,[†] Claudia M. Grozea,[†] Guojun Liu,*[,†] Yu Wang,[†] Alison Crumblehulme,[‡] and Martin Wyer[‡]

[†]Department of Chemistry, Queen's University, 90 Bader Lane, Kingston, Ontario, Canada K7L 3N6

[‡]Lorama Inc., 221 Nipissing Road, Milton, Ontario, Canada L9T 1R3

Supporting Information

ABSTRACT: Two poly[3-(triisopropyloxysilyl)propyl methacrylate]-*block*-poly[2-(perfluorooctyl)ethyl methacrylate] (PIPSMA-*b*-PFOEMA) samples and one poly(perfluoropropylene oxide)-*block*-poly-[3-(triisopropyloxysilyl)propyl methacrylate] (PFPO-*b*-PIPSMA) sample were synthesized, characterized, and used to coat glass plates. These coatings were formed by evaporating a dilute polymer solution containing HCl, which catalyzed PIPSMA's sol–gel chemistry. Polymer usage was minimized by targeting at diblock copolymer unimolecular (brush) layers that consisted of a sol–gelled grafted PIPSMA layer and an oil- and water-repellant fluorinated surface layer. Investigated is the effect of varying the catalyst amount, polymer amount, as well as block copolymer type and composition on the structure, morphology, and oil- and water-repellency of the coatings. Under optimized conditions, the prepared coatings were optically clear and resistant to writing by a permanent marker. The marker's trace was the faintest on PFPO-*b*-PIPSMA coatings. In addition, the PFPO-*b*-PIPSMA coatings were far more wear-resistant than the PIPSMA-*b*-PFOEMA coatings.

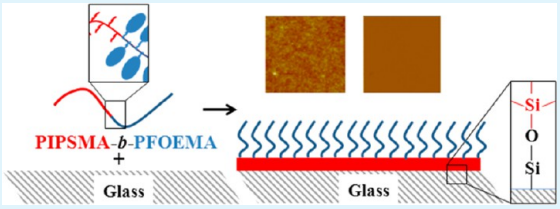

KEYWORDS: *coatings, block copolymer, sol–gel chemistry, oil repellency, and water repellency*

1. INTRODUCTION

Coatings that repel oil- and water-borne contaminants alike are antismudge. Antismudge coatings are currently prepared from three approaches. In approach 1, fluorinated nano- and/or microarchitectures make up the coating.[1−8] While fluorination is used to decrease the surface tension, nano- and micro-architectures are utilized to render the high-surface-area (roughness) and re-entrant features needed for the beading or nonwetting of a testing liquid.[9−11] Coatings prepared through the second approach consist of a porous matrix, such as a fluorinated sponge, that is filled with a fluorinated oil such as a perfluoropolyether (PFPE).[12,13] In this case, the oil is held in position because of its affinity for the porous matrix. A test liquid penetrates minimally into the oil because of the incompatibility between the two liquids. Approach 3 bears resemblance to approach 2 and also uses a fluorinated oil. However, the fluorinated oil, such as a PFPE, is covalently grafted onto a substrate.[14−17]

Coatings prepared from approach 1 may be highly water- and oil-repellant (superamphiphobic) and possess static contact angles exceeding 150° even for hexadecane, which has a room-temperature surface tension of 27.5 mN/m.[18] Liquid droplets are suspended in this case by protrusions of an architectural coating in the Cassie state and readily roll off from the surface because the contact area and thus the van der Waals adhesion forces between the two are small.[1−11] The drawbacks of these rough coatings are their lack of optical clarity and wear resistance.

On a flat coating prepared via approaches 2 or 3, the contact angles of a test liquid such as water or hexadecane never exceed ∼120°.[12−17] However, a test droplet still slips readily off this surface if the coating is thick enough to fully shield the substrate or other functionalities that may pin the test droplet. This is because the van der Waals forces between a fluorinated oil and a test droplet are weak. Moreover, the detachment of an adsorbed droplet is facilitated by the constant molecular motion of fluorinated oil. Furthermore, being flat and physically homogeneous, the coating has no "permanent" solid obtrusions to pin a test droplet. Thus, a droplet on such a coating has a small contact angle hysteresis expressed as $(\cos \theta_R - \cos \theta_A)$, where θ_R and θ_A are the respective receding and advancing contact angles of the test liquid. In this scenario, the droplet would be in the "dynamic nonwetting" regime, and would readily slide off a surface.[19,20]

A PFPE coating prepared via approach 3 is normally a unimolecular layer and is thus thin and optically clear. A clear and antismudge coating may have many applications. For example, if such a coating is applied onto the windows of skyscrapers, it should reduce the frequency of window washing and save cleaning costs. On the touch screen of smart phones or tablets it rejects fingerprints and maintains the display quality and aesthetic appeal of the device. Because of these potential

Received: September 19, 2014
Accepted: November 17, 2014
Published: November 17, 2014

Scheme 1. Chemical Structures of the Copolymers Used in This Study

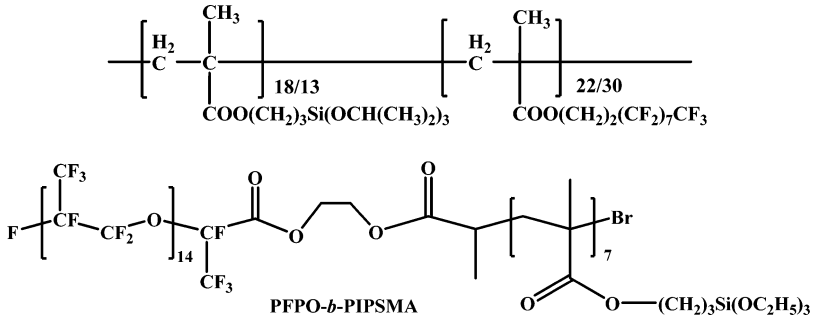

applications, fluorinated polymers such as PFPE bearing one terminal trialkoxysilane group (denoted as -Si(OR)$_3$) have been synthesized and grafted onto glass plates via the sol−gel chemistry of -Si(OR)$_3$.[14,15] However, the use of PFPE-Si(OR)$_3$ produces fewer than three Si−O−Si bonds per grafted PFPE chain. Thus, grafted PFPE-Si(OR)$_3$ chains are less wear resistant than grafted (RO)$_3$Si-PFPE-Si(OR)$_3$ chains, where each PFPE chain was grafted by two -Si(OR$_3$)$_3$ groups at the opposite ends of the chain.[21] We imagined that the wear resistance of a grafted fluorinated layer can also be improved by using diblock copolymers FL$_n$-*b*-GX$_m$ that comprise a fluorinated block of *n* FL units and a grafting/cross-linking block of *m* GX units. In this case, a GX block rather than a single -Si(OR)$_3$ group is used to graft a fluorinated chain and thus the grafting reaction should be more facile. Furthermore, an anchored layer consisting of a GX block should be more stable than a layer derived from -Si(OR)$_3$. Thus, we report in this paper the preparation of FL$_n$-*b*-GX$_m$ brush layers that are grafted onto glass plates. In addition, we report the results of our systematic study on factors such as the amount of polymer and the catalyst as well as the copolymer structure that affect this preparation and the properties of the resultant coatings.

The specific FL$_n$-*b*-GX$_m$ samples that we used are PIPSMA$_{18}$-*b*-PFOEMA$_{22}$ (P1−1), PIPSMA$_{13}$-*b*-PFOEMA$_{30}$ (P1−2), and PFPO$_{14}$-*b*-PIPSMA$_7$ (P2), where the subscripts denote the repeat unit numbers for the different blocks. In addition, PFPO denotes poly(perfluoropropylene oxide), a PFPE, PIPSMA denotes poly(3-(triisopropyloxysilyl)propyl methacrylate), and PFOEMA represents poly(2-(perfluorooctyl)ethyl methacrylate) (Scheme 1). The PIPSMA-*b*-PFOEMA samples were studied because a PIPSMA-*b*-PFOEMA sample has previously been used to coat silica and cotton textiles to yield superamphiphobic coatings.[5,22−25] Two samples, P1−1 and P1−2, of the PIPSMA-*b*-PFOEMA family were used to examine the effect of varying the block length ratio on the surface properties of the coatings. The PIPSMA-*b*-PFOEMA and PFPO-*b*-PIPSMA families were utilized to investigate how the flexibility of the fluorinated block affected the coating properties. While PFOEMA forms a smectic-A liquid crystalline phase at room temperature[26] and has a smectic-A-to-disorder transition temperature of 76 °C,[27,28] PFPO is a liquid at room temperature and has a glass-transition temperature of −71 °C.[29]

2. EXPERIMENTAL SECTION

Materials. α,α,α-Trifluorotoluene (TFT, 99+%, Acros), tetrahydrofuran (THF, 99.9%, Fisher Scientific), sulfuric acid (H_2SO4, 18 M, Fisher), and hydrogen peroxide (H_2O_2, 30%, Fisher) were used as received. Aqueous hydrogen chloride (HCl, 13 M, Fisher) was diluted with THF before use.

Polymer Characterization. Molecular weights were obtained at 40 °C using a Waters 515 size exclusion chromatograph (SEC) that was equipped with a 2419 differential refractive index detector. TFT was used as the mobile phase at a flow rate of 1.00 mL/min. The column used was filled with 5 μm 1000 Å AM gel from the American Polymer Standards Corporation and calibrated with monodisperse polystyrene standards. ^{1}H NMR analysis was performed in $CDCl_3$/C_6F_6 at v/v = 3/2 for P1−1 and P1−2 but in $CDCl_3$/TFT at v/v = 1/3 for P2 on a Bruker Advance 400 MHz spectrometer.

Glass Coating. A Piranha solution (4/1 v/v concentrated H_2SO_4/30% H_2O_2) was used to clean glass plates with dimensions of ∼1.0 × 1.3 cm^2. ***Caution**: Piranha solution is a very strong oxidant.* The plates were then rinsed with water and methanol before they were dried under nitrogen gas. To coat a glass plate, it was placed in a weighing bottle. Dispensed onto it sequentially were 62 μL of TFT, 1.0−3.0 μL of a diblock copolymer solution at 1.0 mg/mL in TFT, and 27 μL of a HCl solution in THF. The HCl solution was prepared by diluting an aqueous HCl solution (13 M) with THF to the concentrations of 3.0 × 10^{-1}, 3.0 × 10^{-2}, 3.0 × 10^{-3}, and 3.0 × 10^{-4} M depending on the desired solution acidity. The volume of the polymer coating solution and the HCl concentration in THF were varied to examine the effect of changing the polymer and the catalyst amount on the properties of the resultant coatings. The weighing bottle was then covered with its lid and ∼19 h was required to evaporate the solvent. The polymer amount used for each sample was adjusted based on the exact area of the glass plate.

PIPSMA Sol−Gel Samples. Two PIPSMA solutions in THF at 10.0 mg/mL were prepared. To one of these 1.0 mL solutions was added 0.050 mL of a HCl solution in THF at 6.2 × 10^{-1} M, and to the other was added 0.010 mL of an HCl solution at 1.0 × 10^{-3} M. Samples were collected at 50 μL of each time from these mixtures before or at different times after HCl addition. These aliquots were directly added to 0.12 g of KBr that was previously ground into a powder using a mortar and pestle. The components were mixed together with a plastic spatula, and the THF was left to evaporate out of the sample for 30 min to yield a dry powder for DRIFT-IR analysis.

Analytical Techniques. The UV−vis transmittance spectra of clean and coated glass plates were recorded using a PerkinElmer Lambda XLS+ spectrometer. Atomic force microscopy (AFM) height and phase images were obtained using a Veeco Multimode instrument equipped with a Nanoscope IIIa controller operated in the Tapping Mode. Rectangular-shaped silicon probes (AppNano, ACT) with a 300 kHz resonance frequency and a spring constant of 40 N/m were used.

XPS measurements were performed using a Thermo Instruments Microlab 310F surface analysis system equipped with an Mg Kα X-ray source (1253.6 eV). An anode potential of 15 kV and an emission current of 20 mA was used. Spectra were acquired in the fixed analyzer transmission mode with a pass energy of 20 eV and a surface/detector takeoff angle of 20°. All spectra were calibrated to the C_{1s} line located at 285.0 eV.

Static, advancing, and receding angles as well as sliding angles were measured at room temperature (21−23 °C) for deionized water, diiodomethane (>99%, Aldrich), and hexadecane (>99%, Aldrich) on coatings. These were measured using a Dataphysics OCA 15 Pro

optical contact angle measuring system. The sliding angle was measured as the angle at which a droplet that was placed on a sample would completely roll off its surface. Static, advancing, and receding contact angles were measured using 5.0 μL droplets and sliding angles were measured using 20 μL droplets at three different positions on each sample.

Durability and Antismudge Properties. The antismudge properties of the coated glass plates were tested using a permanent black marker (Sharpie). The marker was used to write on the coated glass plates. The removal of the dried writing was attempted by rubbing it with a light-duty tissue wiper (VWR).

For the wearing test, a homemade mechanical device was used. The device has a rectangular sample stage made of a wooden plate suspended by four springs and held in position by four sliding posts at its corners. A coated glass plate at the area of ~1.3 cm^2 was glued to the center of the stage. Pressed against the coated plate was a circular cotton-covered probe with a diameter of 4.0 cm. The probe was attached to a mechanical stirrer so that it could be rotated. Typically, a rotation speed of 40 rpm was used for the rubbing test. The force exerted on a coated sample was increased by lowering the position of the probe and was typically set at 4.9 N (pressure was at 3.8×10^4 Pa). Water static contact angles were measured for a given sample after different rubbing cycles to evaluate the effect of rubbing on the deterioration of the surface properties.

3. RESULTS AND DISCUSSION

Diblock Copolymers. P1−1 and P1−2 were synthesized by sequential atom transfer radical polymerization (ATRP).[24,30,31] ATRP was also used to prepare the second block of P2. To prepare P2, a macroinitiator was first prepared from PFPO−COOH, which was PFPO bearing one terminal carboxyl group. The details for the synthesis of these polymers are described in the Supporting Information.

The polymers were characterized by ^{1}H NMR and size exclusion chromatography (SEC) (see Table 1). For ^{1}H NMR analysis of P1−1 and P1−2, $CDCl_3/C_6F_6$ at v/v = 3/2 was used as the solvent. The solvent was changed to $CDCl_3$/TFT at v/v = 1/3 for P2 analysis. ^{1}H NMR analysis yielded the block length ratios n/m. In addition, it yielded the absolute repeat unit numbers for the PIPSMA blocks of P1−1 and P1−2 from the integral ratios between the PIPSMA signal at 0.6 ppm and a characteristic initiator peak at 4.1 ppm (see Figure S4 in the Supporting Information). From ^{1}H NMR analysis we obtained the repeat unit numbers of 18 and 22 for the first and second blocks of P1−1. These values were 13 and 30 for P1−2. The repeat unit number for the PFPO block of P2 was given by the Supplier to be 14. The repeat unit number for the PIPSMA block was determined from ratioing the integrals of IPSMA peaks with that of a macroinitiator peak at 4.6 ppm to be 7 (see Figure S3 in the Supporting Information).

Table 1. Characteristics of the Diblock Copolymers Used

sample	SEC M_n (g/mol)	SEC M_w/M_n	NMR n	NMR m
P1−1	17 600	1.14	18	22
P1−2	19 400	1.12	13	30
P2	4500	1.10	14	7

For SEC analysis, TFT was used as the eluant. The SEC instrument was calibrated using polystyrene standards. Thus, only approximate polydispersity indices (M_w/M_n) and the number-average molecular weights (M_n) were obtained. The samples had low M_w/M_n values.

Glass Coating. Glass plates of an area of ~1.3 cm^2 were coated. To coat a plate, it was leveled inside a weighing bottle. Placed on it were then 62 μL of TFT, 1−3 μL of a 1.0 mg/mL diblock copolymer solution in TFT, and 27 μL of an HCl solution in THF. HCl was used to trigger the sol−gel chemistry of the PIPSMA block of P1−1, P1−2, or P2. Subsequently, the lid was placed onto the weighing bottle to slow down solvent evaporation so that the silanol groups produced had enough time to graft onto the glass plate and the grafted copolymer chains had enough time to organize into a brush layer. Since this coating technology was targeted at practical applications and heating a coated smart phone, for example, in an oven was deemed impractical, the coatings were not further heated.

Effect of Varying [HCl] on the Coating Properties. We examined various factors that affected the coating process. The effect of varying [HCl] on the morphology, surface composition, and amphiphobicity of coatings formed was investigated by AFM, XPS, and contact/sliding angle measurements. Figure 1 shows typical AFM topography and phase images of P1−2 coatings prepared at the fixed polymer amount of 1.95 $\mu g/cm^2$ but at different [HCl] in the final coating solution mixture.

The phase images of the coatings prepared at [HCl] = 9.0×10^{-2} and 9.0×10^{-3} M were homogeneous, suggesting the existence of only one species on the glass surface. Moreover, their topography images were smooth with the root-mean-square roughness (R_{rms}) values of 0.42 and 0.38 nm, respectively, which were comparable to 0.28 nm measured for uncoated glass (see Figure S7 in the Supporting Information). However, more surface bumps were observed when [HCl] was decreased to 9.0×10^{-4} or 9.0×10^{-5} M. This increase in surface roughness was accompanied by the appearance of contrast in the phase images, alluding to more than one species on the coating surface in these cases.

To gain insight into the AFM results, we obtained XPS data for these coatings prepared at [HCl] = 9.0×10^{-2} and 9.0×10^{-5} M, respectively, and the data are shown in Figure 2. The survey XPS spectra clearly show that the area ratio between the F_{1s} and C_{1s} peaks or the relative content between F and C increased when [HCl] was increased from 9.0×10^{-5} to 9.0×10^{-2} M. This conclusion was further supported by the high-resolution spectra of the two coatings in the C_{1S} region shown in Figure 2b. At [HCl] = 9.0×10^{-2} M, the CF_2 and CF_3 contents probed by XPS increased relative to carbonyl carbon or carbon atoms bonded with hydrogen. We further obtained atomic compositions for the surfaces of the two P1−2 coatings and the results are shown in Table 2. When [HCl] was increased from 9.0×10^{-5} to 9.0×10^{-2} M, the F atomic fraction increased from 18.9 to 54.0%, whereas the C, O, and Si fractions decreased from 59.5, 15.7, and 5.9% to 32.1, 11.3, and 2.6%, respectively.

That the F content of 54.0% for the coating prepared at [HCl] = 9.0×10^{-2} M was comparable with 51.5% calculated from the PFOEMA formula because the surface was essentially fully covered by PFOEMA. This concludion agreed with the homogeneous AFM phase images obtained for this coating. The F content of 54.0% was even higher than 51.5%, probably because the perfluorooctyl ethyl groups stretched away from the coating into the air. Previous studies have concluded that the perfluorooctyl ethyl groups formed a liquid crystalline layer on PFOEMA surfaces.[5,26,27]

The coating prepared at [HCl] = 9.0×10^{-5} M had 18.9% F because the PIPSMA chains also occurred on the surface. We have performed a Fourier-trasform infrared analysis of products obtained from treating a PIPSMA homopolymer with HCl at

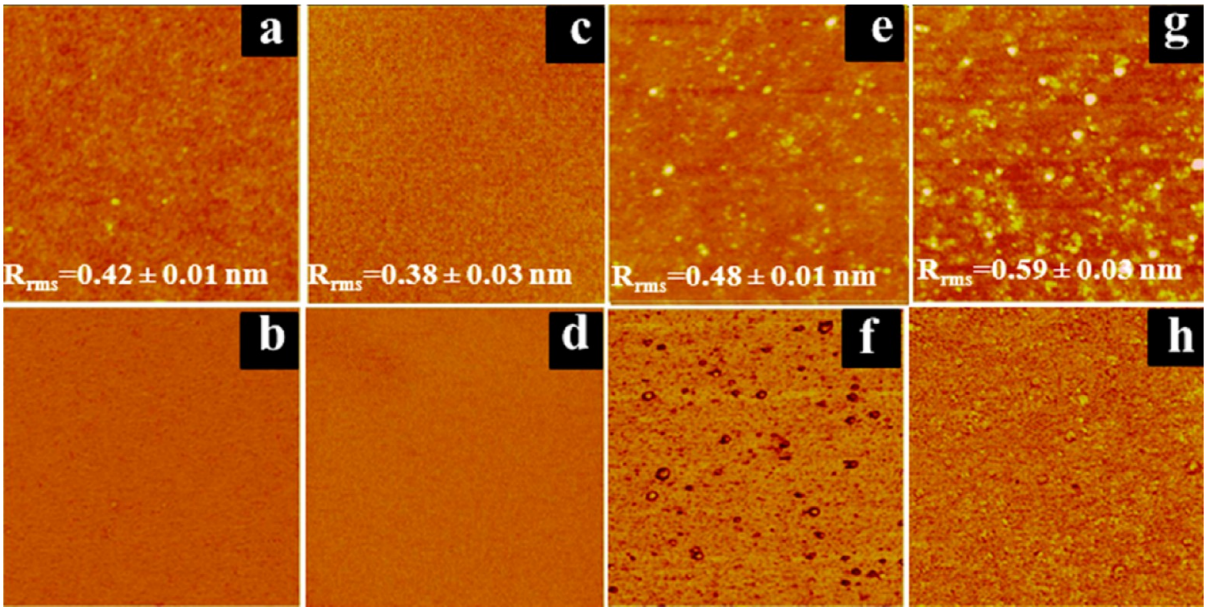

Figure 1. AFM (top row) height and (bottom row) phase images of P1−2 coatings prepared at 1.95 μg/cm^2 but different [HCl]: (a, b) 9.0×10^{-2} M, (c, d) 9.0×10^{-3} M, (e, f) 9.0×10^{-4} M, and (g, h) 9.0×10^{-5} M. The height and phase angle ranges are 20 nm and 75°, respectively, and the image areas are 2.0×2.0 μm^2.

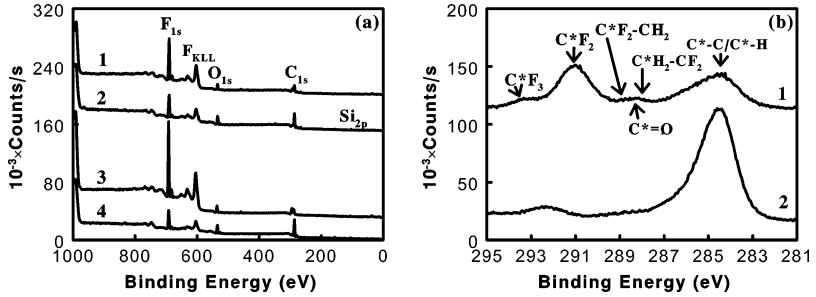

Figure 2. (a) XPS survey spectra of P1−1 and P1−2 coatings prepared at 1.50 and 1.95 μg/cm^2: (1, 2) P1−1 coatings prepared at [HCl] = 9.0×10^{-2} and 9.0×10^{-5} M, respectively. (3, 4) P1−2 coatings prepared at [HCl] = 9.0×10^{-2} and 9.0×10^{-5} M, respectively. (b) High-resolution C_{1S} spectra of P1−2 coatings prepared at: (1) [HCl] = 9.0×10^{-2} M and (2) at [HCl] = 9.0×10^{-5} M.

Table 2. Surface Atomic Compositions Probed by XPS for Various Coatings

			atomic concentration (%)			
sample	[HCl] (M)	polymer amount (μg/cm^2)	C	F	O	Si
P1−1	9.0×10^{-2}	1.50	51.4	36.9	9.1	2.5
P1−1	9.0×10^{-5}	1.50	61.4	21.2	13.4	4.0
P1−2	9.0×10^{-2}	1.95	32.1	54.0	11.3	2.6
P1−2	9.0×10^{-5}	1.95	59.5	18.9	15.7	5.9
P2	9.0×10^{-2}	1.50	34.2	45.0	15.7	5.1

various concentrations for different times and discovered that PIPSMA did not sol−gel at [HCl] ≈ 9.0×10^{-5} M after 2 h (see Figure S9 in the Supporting Information). Thus, the PIPMA block of P1−2 did not effectively graft onto glass and could occur in the surface layer. This premise agreed with the observation of contrast in AFM phase images of this sample. The structural difference for coatings prepared at different [HCl] was also confirmed by their differnet wetting properties. We measured the static, advancing (θ_A), and receding (θ_R) contact angles of water, diiodomethane, and hexadecane on P1−2 coatings prepared at 1.95 μg/cm^2 and different [HCl]. We also measured the sliding angles above which a 20 μL droplet slid off a coated glass plate. Some of these data as well as the cos θ_R − cos θ_A results are plotted in Figure 3. The cos θ_R − cos θ_A values were plotted as they dictate the readiness for a droplet to slide.[19,32] As [HCl] decreased, the contact angles, the hysteresis (θ_A − θ_R), the sliding angles, and the cos θ_R − cos θ_A values increased, suggesting a deterioration in coatings' repellency. Therefore, these static and dynamic wetting data were consistent with a decreasing fluorine content on the coating surfaces as [HCl] decreased.

We also obtained XPS atomic compositions of P1−1 coatings prepared at 1.50 μg/cm^2 but [HCl] = 9.0×10^{-2} and 9.0×10^{-5} M, respectively. The atomic composition variation trends with [HCl] (Table 2) mirrored those observed for the P1−2 coatings. In a further experiment, we extracted the P1−1 and P1−2 coatings prepared at [HCl] = 9.0×10^{-2} M in TFT overnight, no changes in water contact angles were observed, confirming the covalent attachment of the coatings prepared at [HCl] = 9.0×10^{-2} M. Therefore, all coatings to be discussed hereon were prepared at [HCl] = 9.0×10^{-2} M.

Dynamic Nonwetting Properties. Videos were taken of water and hexadecane droplets on a P1−2 coating prepared under optimized conditions, which used [HCl] = 9.0×10^{-2} M

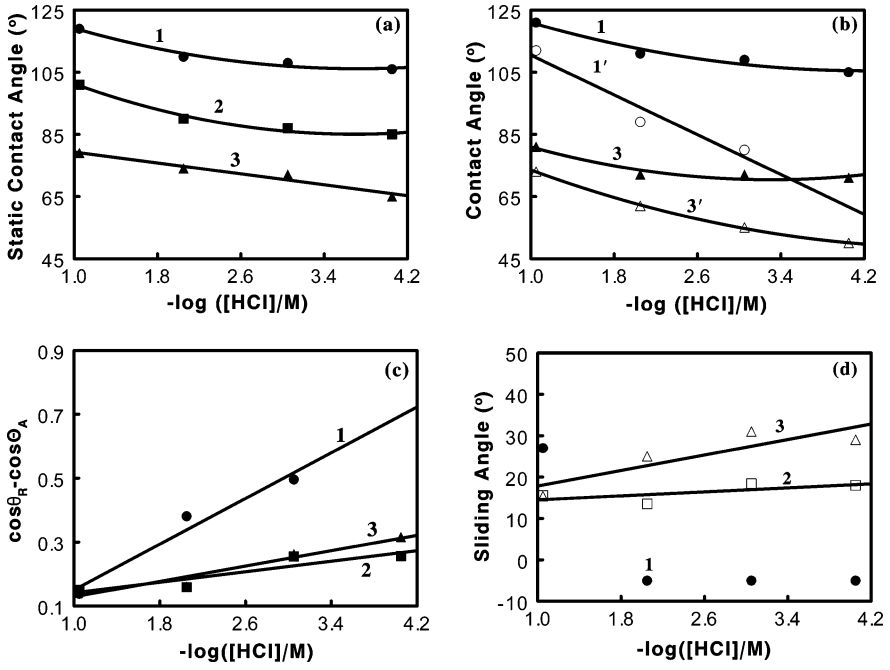

Figure 3. Effect of varying [HCl] on the static and dynamic wetting properties of P1−2 coatings prepared at a polymer amount of 1.95 μg/cm^2: (a) Static contact angle variation for (1) water, (2) diiodomethane, and (3) hexadecane. (b) Advancing and receding angle variation for (1 and 1′) water and (3 and 3′) hexadecane. (c) (cos θ_R − cos θ_A) variation for (1) water, (2) diiodomethane, and (3) hexadecane. (d) Sliding angle variation for 20 μL droplets of (1) water, (2) diiodomethane, and (3) hexadecane. Negative sliding angles indicated that water droplets did not slide off the glass plates.

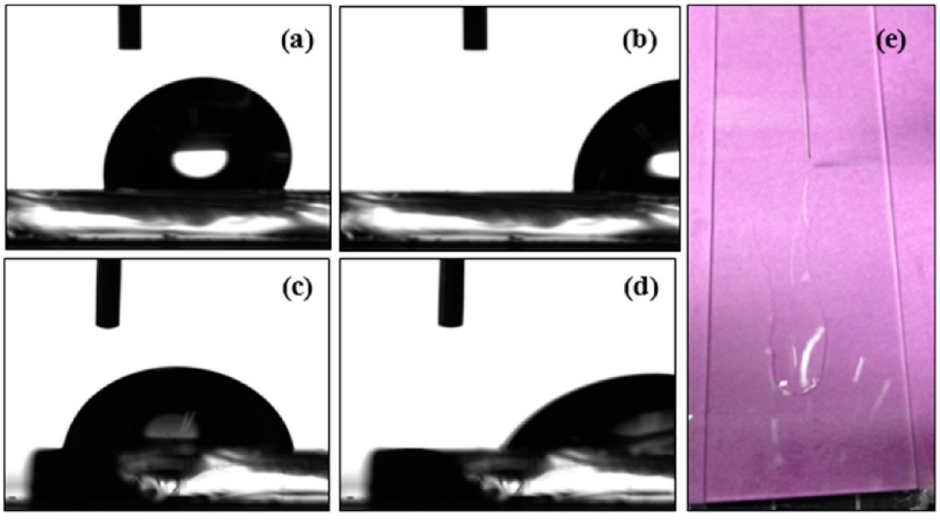

Figure 4. Photographs of (a, b) water and (c, d) hexadecane droplets after being dispensed onto P1−2-coated glass plates. The time lag between a and b was 17 s and that between c and d was 9 s. The dark cylindrical object at the top left corner of each photograph was the stationary syringe needle tip. Long times were required before the droplets moved because the plate slanting angles were gradually increased to 30 and 19° for water and hexadecane, respectively. (e) On an uncoated glass plate, hexadecane spread rather than slid.

and a polymer amount of 1.95 μg/cm^2, as the glass plate slanting angle was gradually increased from 0° to the final values of 30 and 19°, respectively. Figure 4 shows snapshots of the water and hexadecane droplets. The droplet contact angles as seen in Figure 4 are lower than 120°. However, no liquid residue was left behind after a liquid droplet glided down a coated glass plate. Thus, the coating manifests its repellency not in high droplet contact angles but in the sliding down of the droplets in whole. In contrast, a hexadecane droplet spread on an uncoated slanted glass plate and its traveled path was marked by oil streaks.

Effect of Varying the Polymer Amount. We imagined that insufficient P1−2 coated at [HCl] = 9.0 × 10^{-2} M would yield "patches" or "islands" on the glass surface. Increasing the P1−2 amount would first produce a loosely packed P1−2 layer and eventually a crowded brush layer. In a crowded brush layer, the sol−gelled PIPSMA block would graft and cross-link on the glass and the PFOEMA block would stretch into the solvent phase.[33−38] Of course, the PFOEMA chains would eventually collapse after solvent evaporation. Increasing the P1−2 amount beyond that required for a saturated brush would produce also some nanoclusters on the brush surface. These clusters should

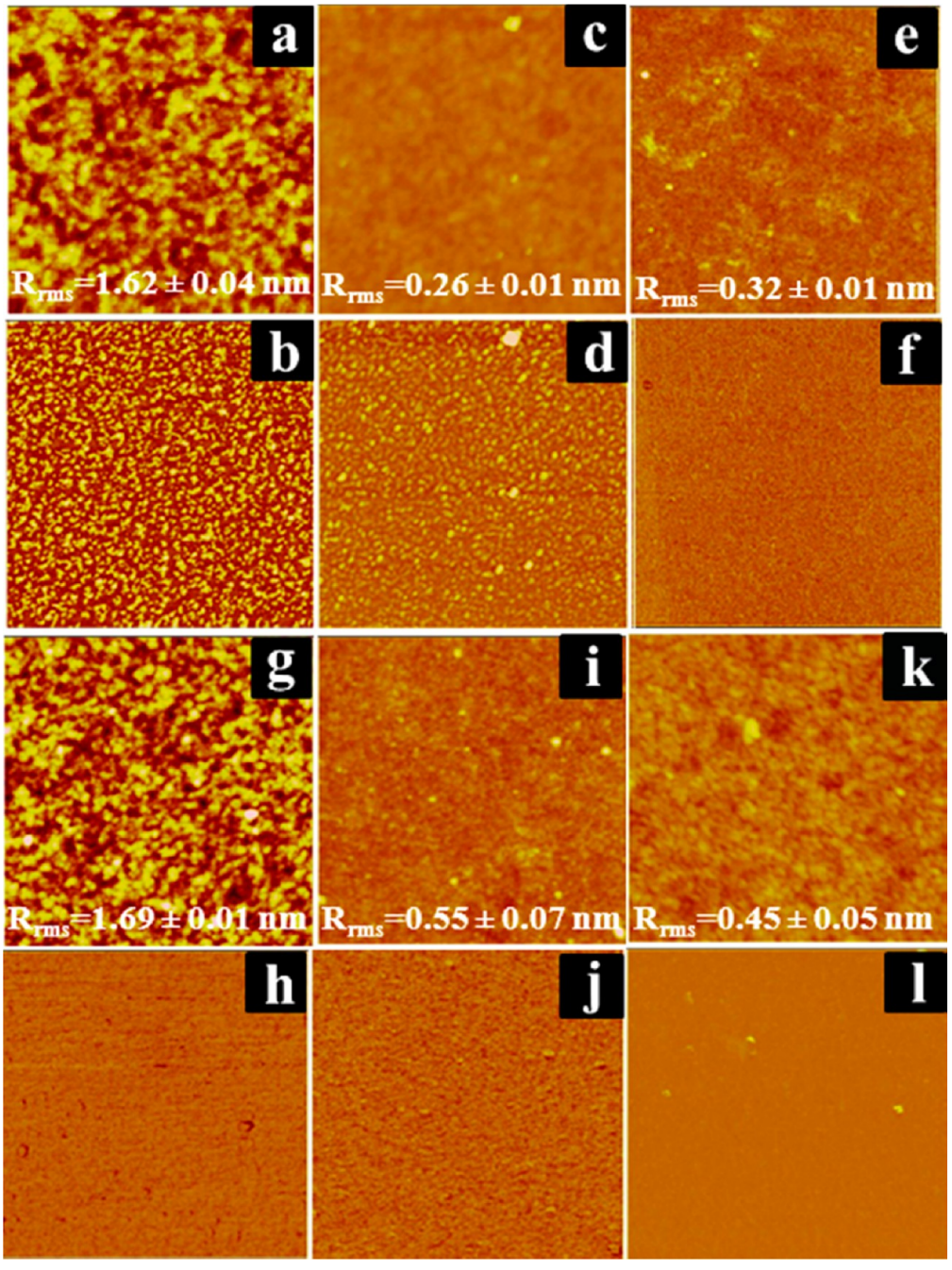

Figure 5. (a–h) AFM height and phase images for P1–2 coatings prepared at [HCl] = 9.0×10^{-2} M but different polymer amounts. The polymer amounts were (a, b) 0.76, (c, d) 1.15, (e, f) 1.62, and (g, h) 2.31 μg/cm^2, respectively. (i–l) AFM topography and phase images for (i, j) P1–1 and (k, l) P2 coatings prepared at [HCl] = 9.0×10^{-2} M and the polymer amount of 1.50 μg/cm^2. The height and phase angle delay ranges were 20 nm and 75° and the images sizes were 2.0 × 2.0 μm^2. The topography images are marked by their R_{rms} values.

have a sol–gelled PIPSMA core surrounded by a PFOEMA corona. Because they were physically deposited onto the brush layer, they could be easily removed and would not contribute to the long-term amphiphobicity. Therefore, we targeted amphiphobic coatings composed of a saturated brush layer, which should provide optimal amphiphobicity using a minimal amount of a fluorinated copolymer.

To estimate the P1–2 amount required to form a saturated brush layer, we used the fully stretched length of 12.2 nm for a chain consisting of 13 PIPSMA units and 30 PFOEMA units. Using the average density of 1.85 g/cm^3 for the PFOEMA and sol–gelled PIPSMA blocks (see section 4 in the Supporting Information), we estimated that 2.67 μg of P1–2 was required to prepare a sol–gelled film that was 12.2 nm thick and had an area of 1.3 cm^2. In reality, the polymer in a brush layer could not be as dense as a solid polymer. Thus, we used P1–2 amounts typically less than this number to achieve a brush coating.

Figure 5 compares the AFM topography and phase images of P1–2 coatings prepared at the polymer amounts of 0.76, 1.15, 1.62, and 2.31 μg/cm^2, respectively. These images and those shown in Figure 1 prepared at 1.95 μg/cm^2 suggest the following trend. At a low polymer amount of 0.76 μg/cm^2, the coating was rough as revealed by the topography image (Figure

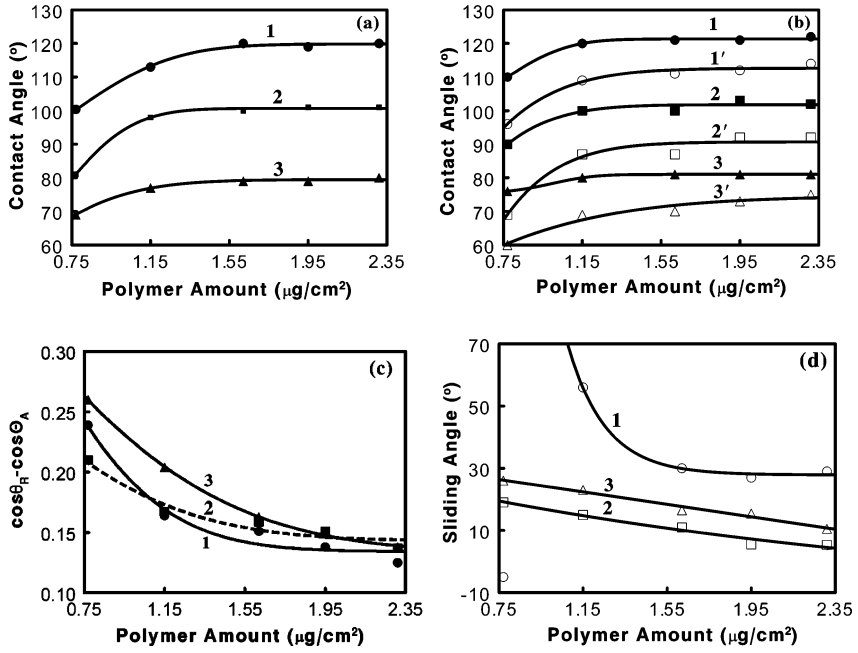

Figure 6. Effect of varying the polymer amount on the static and dynamic wetting properties of P1−2 coatings prepared at [HCl] = 9.0×10^{-2} M: (a) Static contact angle variation for (1) water, (2) diiodomethane, and (3) hexadecane. (b) Advancing and receding angle variation for (1 and 1′) water, (2 and 2′) diiodomethane, and (3 and 3′) hexadecane. (c) ($\cos\theta_R - \cos\theta_A$) variation for (1) water, (2) diiodomethane, and (3) hexadecane. (d) Sliding angle variation for 20 μL droplets of (1) water, (2) diiodomethane, and (3) hexadecane. The negative sliding angle in d suggests that the water droplets did not slide off the glass plates.

5a). The phase image shown in Figure 5b suggested that the coated glass plate was chemically heterogeneous. As the polymer amount was increased, the surface composition heterogeniety as revealed by the phase images decreased. The surface roughness initially decreased with the polymer amount. As the polymer amount reached 2.31 $\mu g/cm^2$, the surface became rough again despite the homogeneous surface composition, as revealed by the phase image.

The image variation trend supported our proposed effect of varying the polymer amount on the coating structure. The surface was rough at low P1−2 amounts because only a patchy submonolayer was formed. Since only certain regions of the glass plate were covered by P1−2, two types of surfaces, glass vs polymer, were probed by AFM in the phase mode. Above a certain polymer amount, the glass was fully covered by P1−2. Thus, the surface roughness and phase contrast decreased. Increasing the P1−2 amount beyond what was needed for a saturated monolayer produced not only a brush layer, but also some nanoclusters. Thus, the surface roughness increased again. Because both the nanoclusters and the brush layer had a PFOEMA surface, the surface composition as probed by phase-mode AFM remained homogeneous.

The surface compositional homogeniety above a certain P1−2 amount was supported by the static and dynamic wetting properties determined for the coated glass (Figure 6). The static, advancing, and receding angles of the three testing liquids (water, diiodomethane, and hexadecane) all increased initially with the P1−2 amount. Above 1.65 $\mu g/cm^2$, these angles plateaued. In addition, the hysteresis and the $\cos\theta_R - \cos\theta_A$ values initially decreased and then plateaued above 1.65 $\mu g/cm^2$. This plateauing trend was reflected by the sliding angle data for water as well.

P1−1 and P2 were also used to fluorinate glass plates. To ensure a saturated brush layer in each case, we used the polymer amount of 1.50 $\mu g/cm^2$ for P1−1 or P2. This amount was less than 1.95 $\mu g/cm^2$ used for P1−2 because P1−2 had the longest chains and the highest molecular weight among the three reagents and should form the thickest brush coating. We confirmed that 1.50 $\mu g/cm^2$ was sufficient for a saturated P1−1 brush by comparing static water contact angles on coatings prepared at 1.50 and 2.00 $\mu g/cm^2$, respectively. The contact angles were the same at 115 ± 2° on the two types of coatings.

Representative AFM topography images of glass plates coated by P1−1 and P2 are shown in Figure 5. Both coatings were smooth with low R_{rms} values. The P1−1 and P2 coatings were also analyzed by XPS. According to Table 2, the P1−1 coating had the following atomic composition: C = 51.4% and F = 36.9%. The F content was lower than 54.0% determined for P1−2 coatings. We suspect that the differences were caused by the reduced ability of the thin PFOEMA layer in a P1−1 brush to block the XPS electrons from reaching the underlying sol−gelled PISPMA block and the glass. XPS analysis of the P2 coatings yielded the following atomic compositions: C = 34.2%, F = 45.0%, O = 15.7%, and Si = 5.1%. The PFPO component of P2 (Scheme 1) has the formula of $C_{44}F_{89}O_{14}$ (H excluded) and thus the compositions of C = 29.9%, F = 60.5%, and O = 9.5%. The measured F content was lower than that calculated for PFPO, suggesting that the PFPO layer was thin and XPS probed species beneath it.

Coatings of Different Polymers. Glass plates coated at [HCl] = 9.0×10^{-2} M by P1−1 at 1.50 $\mu g/cm^2$, P1−2 at 1.95 $\mu g/cm^2$, and P2 at 1.50 $\mu g/cm^2$ were all optically clear. Between 500 and 550 nm, the transmittances of the coated glass plates were all higher than 89.6%, which was measured for an uncoated glass plate. For glass plates coated by P1−1, P1−2, and P2, the average transmittances were 90.2%, 91.3%, and 91.6%, respectively (Figure 7a). The optical clarity was further confirmed by our ready viewing of writing underneath the coated glass plates (Figure 7b). The transmittance increased for the coated glass plates because the fluorinated polymers had

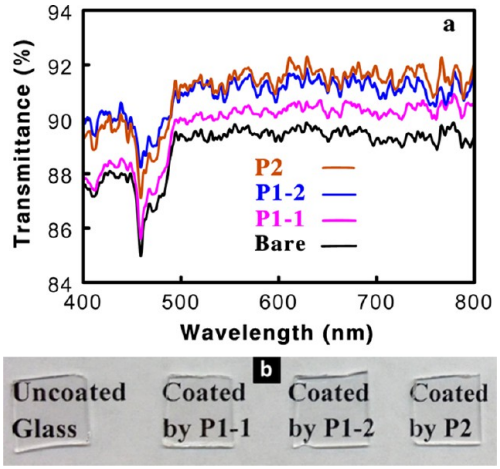

Figure 7. (a) Transmittance curves for an uncoated (bare) glass plate and for glass plates that were coated with P1−1, P1−2, and P2. (b) Photograph of an uncoated glass plate and glass plates coated with different polymers under optimized conditions.

refractive indices between those of glass and air. This gradual refractive index decrease from the glass to air helped suppress light loss due to interfacial reflection.[15,16]

Figure 8 compares the static, advancing, and receding contact angles as well as the cos θ_R − cos θ_A and sliding angle data for water, diiodomethane, and hexadecane on glass substrates coated by different polymers. The P1−2 coatings clearly possessed the highest contact angles and the lowest sliding angles. On the other hand, the P2 coatings had the lowest static contact angles and the highest hysteresis for water droplets. Despite their low static contact angles, the P2 coatings had low cos θ_R − cos θ_A values and sliding angles for diodomethane and hexadecane.

P1−2 coatings were more amphiphobic than P1−1 coatings because P1−2 had a longer PFOEMA block than P1−1. Meanwhile, P2 coatings had lower static contact angles than the P1 coatings because the fluorinated block of P2 differed from those of the P1 polymers. Depending on the molecular weight, PFPO had a surface tension of 17−19 mN/m,[39] which was higher than the value of 6.5 mN/m reported for PFOEMA[40,41] and the liquids are supposed to have lower contact angles on PFPO. Despite the lower static contact angles, the (cos θ_R − cos θ_A) values of diiodomethane and hexadecane were low on the P2 coatings because PFPO is an oil and possesses good dynamic dewetting properties, a phenomenon that has been well-documented previously.[15,17,42,43]

A surprise was that the (cos θ_R - cos θ_A) value and sliding angle for water droplets was high on our P2 coatings.[14,15] This was probably due to the thinness of the PFPO layer and its inability to fully shield the underlying sol−gelled hydrophilic PIPSMA layer, which pinned the water droplets and induced hysteresis. We further note that the literature-reported substantially lower sliding angles of 3°[14] and 18°[15] for water were achieved on coatings of a different perfluoropolyether, poly(*n*-perfluoropropylene oxide). Poly(*n*-perfluoropropylene oxide) should have better dynamic dewetting properties than our PFPO because the glass-transition temperature of −101 °C for the former[44] is lower than −71 °C for the latter.[29]

The superior oil repellency of the P2 coatings was further demonstrated by an ink-resistant test, which involved writing on glass plates using a permanent Sharpie oil-based dark marker. On an uncoated glass plate, the lines of ink were evidently thicker than those on plates coated by P1−1 or P1−2 (Figure 9). Intriguingly, the written lines on P2-coated glass plates were seen to shrink within fractions of a second and the final stabilized written lines were much fainter than those left on plates coated by P1−1 or P1−2.

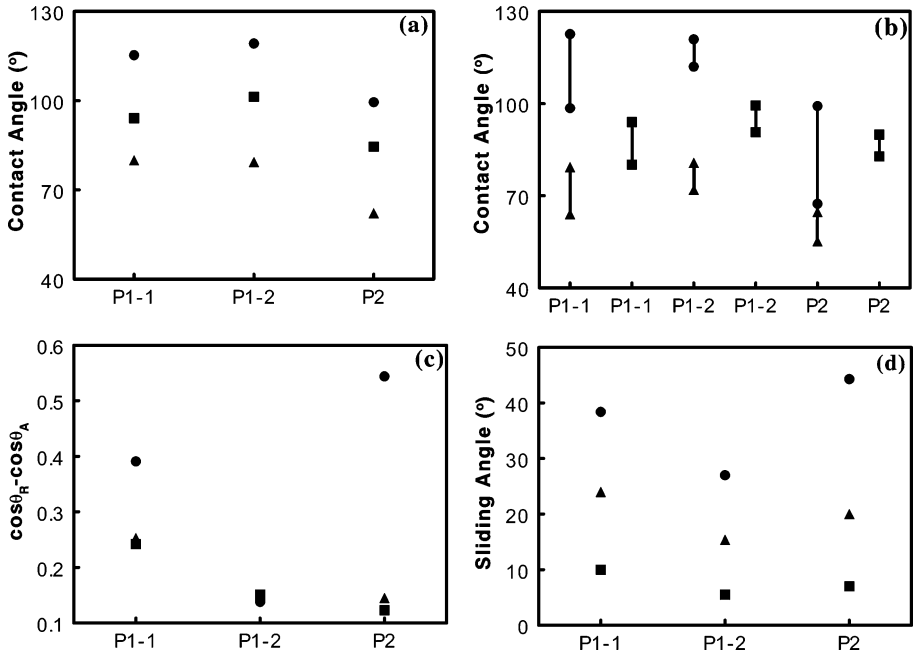

Figure 8. Comparison of the static and dynamic wetting properties of coatings prepared from P1−1, P1−2, and P2 at [HCl] = 9.0×10^{-2} M. (a) Static contact angle variation for (●) water, (■) diiodomethane, and (▲) hexadecane. (b) Variation in (higher value of each pair connected by a line) advancing and receding angle for (●) water, (■) diiodomethane, and (▲) hexadecane. (c) (cos θ_R − cos θ_A) variation for (●) water, (■) diiodomethane, and (▲) hexadecane. (d) Sliding angle variation for 20 μL droplets of (●) water, (■) diiodomethane, and (▲) hexadecane.

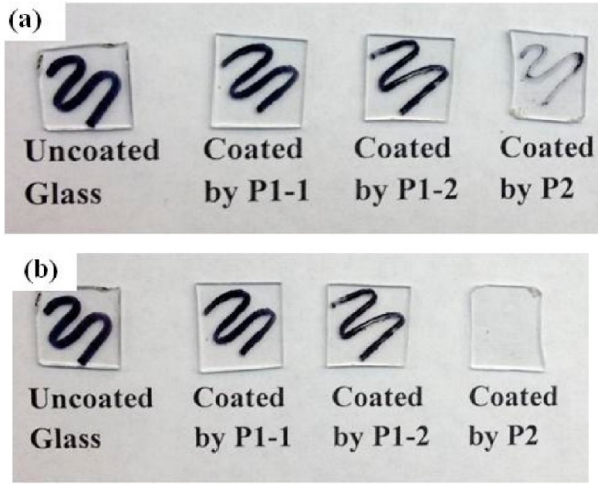

Figure 9. Photographs of an uncoated glass plate and plates that were coated using different polymers: (a) after they had been written on with a black permanent marker and (b) after ink removal with a tissue.

After the written lines were dried, fresh tissue was used to clean the ink. Evidently, the ink could not be readily removed from the uncoated glass plate as they were effectively "permanent". The ink was not readily removed from the plates coated by P1−1 or P1−2 either. In stark contrast, the ink was easily removed from plates coated by P2.

P2-coated plates were not only more resistant against writing, but also writings on P2 coatings were more readily removed. We imagined that the ink easily shrank on a P2-coated glass plate because the PFPO layer is a fluorinated oil.[12] The wriggling motion of its constituent PFPO chains helped gather the ink traces to minimize ink/PFPO contact. The ink was more readily removed again probably because of the mobile nature of the PFPO chains, which helped push the ink patches up from "crevices" that were normally found in a solid substrate. Thus, the dynamic nature of a liquid substrate facilitates the release of the ink and presumably other dirt or smudges.

Wear Resistance. The durability of the polymer coatings was tested using a homemade mechanical device with its photo shown in the Supporting Information (Figure S11). After a P2 coating was rubbed at 3.8×10^4 Pa for 40, 200, and 2400 cycles, the ink from the antiwriting test still shrank readily.

Static water contact angles were also measured on different polymer coatings after they were rubbed for different cycles (Table 3). The P1−1 coatings exhibited the largest decrease in their contact angles after the rubbing treatment. The P1−2 coatings deteriorated at a slower rate. No noticeable deterioration was noticed after rubbing the P2 coatings. The slower deterioration of the P1−2 than the P1−1 coatings should be due to the presence of more fluorinated component on the glass in the former case and thus more time was required to wear the fluorinated component off. The superior wear resistance of the P2 coatings should be due to the slippery properties or the lower friction coefficient of the PFPO layer.[21]

Table 3. Water Static Contact Angles Observed before and after Rubbing Treatment for Various Rubbing Cycles

sample	before rubbing	after 40 cycles	after 200 cycles	after 2400 cycles
P1−1	(115 ± 2)°	(95 ± 2)°	(55 ± 2)°	(50 ± 2)°
P1−2	(118 ± 2)°	(108 ± 2)°	(90 ± 2)°	(90 ± 2)°
P2	(100 ± 2)°	(100 ± 2)°	(100 ± 2)°	(100 ± 2)°

4. CONCLUSIONS

Three diblock copolymers P1−1, P1−2, and P2 have been synthesized and characterized. Mixing a dilute polymer solution in TFT with a HCl solution in THF on a glass plate and slowly evaporating the solvent yielded a diblock copolymer film. At sufficiently high HCl concentrations, e.g. at 0.090 M, a stable layer that resisted overnight extraction by TFT was formed. This stability should be due to sol−gel reactions involving the PIPSMA block and PIPSMA's formation of a grafted and cross-linked layer on the glass plate. The static, advancing, and receding contact angles of water, diiodomethane, and hexadecane droplets increased, and their contact angle hysteresis decreased initially with the deposited polymer amount per unit glass area. However, these values plateaued once the polymer amount apparently exceeded that required for the formation of a saturated diblock brush layer or monolayer. Under optimized coating conditions, the formed monolayers were shown by XPS to have the fluorinated blocks as the surface layers. Additionally, the monolayers were shown by AFM to be smooth and to be clear by spectrophotometric analysis in the visible light region. While P1−2 had higher contact angles and lower droplet sliding angles than P2, P2 had the best resistance against writing by a permanent marker and ink markings immediately shrank into small patches on optimized P2 coatings. After they had been dried, these patches were also readily removed by wiping them with tissue paper, unlike the "permanent" marks that would have remained on uncoated glass. These optically clear amphiphobic diblock copolymer thin layers may serve as coatings for self-cleaning windows of skyscrapers or the touch screens of smart phones and tablets.

■ ASSOCIATED CONTENT

Supporting Information

Synthetic protocols and characterization results for the block copolymers. Theoretical calculations of the maximum film thickness and copolymer amounts required for monolayers. AFM height and phase images of clean glass plates and glass plates coated with P1−2 before and after TFT extraction. DRIFT-IR spectra of sol−gelled PIPSMA samples. Additional XPS survey spectra and high resolution spectra such as C_{1s}, F_{1s}, O_{1s}, or Si_{2p} for PFOEMA, P1−1, and P1−2 are also provided. A graph demonstrating the determination of the water advancing and receding angles on a P1−2 coating and a photograph of the homemade device for wear test are also included. This material is available free of charge via the Internet at http://pubs.acs.org.

■ AUTHOR INFORMATION

Corresponding Author

*E-mail: gliu@chem.queensu.ca.

Notes

The authors declare no competing financial interest.

■ ACKNOWLEDGMENTS

We gratefully thank the Lorama Group and the Collaborative Research and Development program of the Natural Sciences and Engineering Research Council of Canada (NSERC) for sponsoring this research. G.L. thanks the Canada Research

Chair program for a Tier I Canada Research Chair Position in Materials Science.

REFERENCES

(1) Tuteja, A.; Choi, W.; Ma, M. L.; Mabry, J. M.; Mazzella, S. A.; Rutledge, G. C.; McKinley, G. H.; Cohen, R. E. Designing Superoleophobic Surfaces. *Science* **2007**, *318*, 1618−22.

(2) Tuteja, A.; Choi, W. J.; McKinley, G. H.; Cohen, R. E.; Rubner, M. F. Design Parameters for Superhydrophobicity and Superoleophobicity. *MRS Bull.* **2008**, *33*, 752−58.

(3) Deng, X.; Mammen, L.; Butt, H. J.; Vollmer, D. Candle Soot as a Template for a Transparent Robust Superamphiphobic Coating. *Science* **2012**, *335*, 67−70.

(4) Xiong, D. A.; Liu, G. J.; Zhang, J. G.; Duncan, S. Bifunctional Core-Shell-Corona Particles for Amphiphobic Coatings. *Chem. Mater.* **2011**, *23*, 2810−20.

(5) Xiong, D.; Liu, G. J.; Hong, L. Z.; Duncan, E. J. S. Superamphiphobic Diblock Copolymer Coatings. *Chem. Mater.* **2011**, *23*, 4357−66.

(6) Xiong, D. A.; Liu, G. J.; Duncan, E. J. S. Simultaneous Coating of Silica Particles by Two Diblock Copolymers. *ACS Appl. Mater. Interfaces.* **2012**, *4*, 2445−54.

(7) Jiang, W. J.; Grozea, C. M.; Shi, Z. Q.; Liu, G. J. Fluorinated Raspberry-Like Polymer Particles for Superamphiphobic Coatings. *ACS Appl. Mater. Interfaces.* **2013**, *6*, 2628−37.

(8) Xue, Z.; Liu, M.; Lei, J. Recent Developments in Polymeric Superoleophobic Surfaces. *J. Polym. Sci., Part B: Polym. Phys.* **2012**, *50*, 1209−24.

(9) Nosonovsky, M.; Bhushan, B. Roughness-Induced Superhydrophobicity: A Way to Design Non-Adhesive Surfaces. *J. Phys.: Condens. Matter* **2008**, *20*, 2250009.

(10) Zhao, H.; Law, K. Y.; Sambhy, V. Fabrication, Surface Properties, and Origin of Superoleophobicity for a Model Textured Surface. *Langmuir* **2011**, *27*, 5927−35.

(11) Zhao, H.; Park, K. C.; Law, K. Y. Effect of Surface Texturing on Superoleophobicity, Contact Angle Hysteresis, and "Robustness". *Langmuir* **2012**, *28*, 14925−34.

(12) Wong, T. S.; Kang, S. H.; Tang, S. K. Y.; Smythe, E. J.; Hatton, B. D.; Grinthal, A.; Aizenberg, J. Bioinspired Self-Repairing Slippery Surfaces with Pressure-Stable Omniphobicity. *Nature* **2011**, *477*, 443−47.

(13) Yao, X.; Dunn, S. S.; Kim, P.; Duffy, M.; Alvarenga, J.; Aizenberg, J. Fluorogel Elastomers with Tunable Transparency, Elasticity, Shapememory, and Antifouling Properties. *Angew. Chem., Int. Ed.* **2014**, *53*, 4418−22.

(14) Block, S.; Kleyer, D.; Hupfield, P.; Kitaura, E.; Itami, Y.; Masutani, T.; Nakai, Y. New Anti-Fingerprint Coatings. In *11th Annual Coatings for Plastics Symposium*; Paint & Coating Industry: Chicago, 2008; pp 88−92.

(15) Cheng, D. F.; Masheder, B.; Urata, C.; Hozumi, A. Smooth Perfluorinated Surfaces with Different Chemical and Physical Natures: Their Unusual Dynamic Dewetting Behavior toward Polar and Nonpolar Liquids. *Langmuir* **2013**, *29*, 11322−29.

(16) Cheng, D. F.; Urata, C.; Masheder, B.; Hozumi, A. A Physical Approach to Specifically Improve the Mobility of Alkane Liquid Drops. *J. Am. Chem. Soc.* **2012**, *134*, 10191−99.

(17) Cheng, D. F.; Urata, C.; Yagihashi, M.; Hozumi, A. A Statically Oleophilic but Dynamically Oleophobic Smooth Nonperfluorinated Surface. *Angew. Chem., Int. Ed.* **2012**, *51*, 2956−59.

(18) Weast, R. C.; Lide, D. R.; Astle, M. J.; Beyer, W. H. *CRC Handbook of Chemistry and Physics*, 70th ed.; CRC Press: Boca Raton, FL, 1990.

(19) Furmidge, C. G. Studies at Phase Interfaces 0.1. Sliding of Liquid Drops on Solid Surfaces and a Theory for Spray Retention. *J. Colloid Sci.* **1962**, *17*, 309−24.

(20) Fadeev, A. Y.; McCarthy, T. J. Trialkylsilane Monolayers Covalently Attached to Silicon Surfaces: Wettability Studies Indicating That Molecular Topography Contributes to Contact Angle Hysteresis. *Langmuir* **1999**, *15*, 3759−66.

(21) Kondo, H.; Sungkil, L.; Hanaoka, H. Durable Antismudge Materials for Display Terminals. *Triol. Lubr. Technol.* **2009**, *65*, 54−61.

(22) Xiong, D. A.; Liu, G. J.; Duncan, E. J. S. Diblock-Copolymer-Coated Water- and Oil-Repellent Cotton Fabrics. *Langmuir* **2012**, *28*, 6911−18.

(23) Xiong, D. A.; Liu, G. J.; Duncan, E. J. S. Robust Amphiphobic Coatings from Bi-Functional Silica Particles on Flat Substrates. *Polymer* **2013**, *54*, 3008−16.

(24) Shi, Z. Q.; Wyman, I.; Liu, G. J.; Hu, H.; Zou, H. L.; Hu, J. W. Preparation of Water-Repellent Cotton Fabrics from Fluorinated Diblock Copolymers and Evaluation of Their Durability. *Polymer* **2013**, *54*, 6406−14.

(25) Henselwood, F.; Wang, G. C.; Liu, G. J. Removal of Perylene from Water Using Block Copolymer Nanospheres or Micelles. *J. Appl. Polym. Sci.* **1998**, *70*, 397−408.

(26) Al-Hussein, M.; Serero, Y.; Konovalov, O.; Mourran, A.; M?ller, M.; de Jeu, W. H. Nanoordering of Fluorinated Side-Chain Liquid Crystalline/Amorphous Diblock Copolymers. *Macromolecules* **2005**, *38*, 9610−16.

(27) Gao, Y.; Li, X. Y.; Hong, L. Z.; Liu, G. J. Mesogen-Driven Formation of Triblock Copolymer Cylindrical Micelles. *Macromolecules* **2012**, *45*, 1321−30.

(28) Li, X. Y.; Gao, Y.; Xing, X. J.; Liu, G. J. Polygonal Micellar Aggregates of a Triblock Terpolymer Containing a Liquid Crystalline Block. *Macromolecules* **2013**, *46*, 7436−42.

(29) Yarbrough, J. C.; Rolland, J. P.; DeSimone, J. M.; Callow, M. E.; Finlay, J. A.; Callow, J. A. Contact Angle Analysis, Surface Dynamics, and Biofouling Characteristics of Cross-Linkable, Random Perfluoropolyether-Based Graft Terpolymers. *Macromolecules* **2006**, *39*, 2521−28.

(30) Rabnawaz, M.; Liu, G. Preparation and Application of a Dual Light-Responsive Triblock Terpolymer. *Macromolecules* **2012**, *45*, 5586−95.

(31) Rabnawaz, M.; Liu, G. Triblock Terpolymers Bearing a Redox-Cleavable Junction and a Photocrosslinkable Block. *Macromolecules* **2014**, *47*, 5115−23.

(32) Kawasaki, K. Study of Wettability of Polymers by Sliding of Water Drop. *J. Colloid Sci.* **1960**, *15*, 402−07.

(33) Zhao, B.; Brittain, W. J. Polymer Brushes: Surface-Immobilized Macromolecules. *Prog. Polym. Sci.* **2000**, *25*, 677−710.

(34) Stuart, M. A. C.; Huck, W. T. S.; Genzer, J.; Muller, M.; Ober, C.; Stamm, M.; Sukhorukov, G. B.; Szleifer, I.; Tsukruk, V. V.; Urban, M.; Winnik, F.; Zauscher, S.; Luzinov, I.; Minko, S. Emerging Applications of Stimuli-Responsive Polymer Materials. *Nat. Mater.* **2010**, *9*, 101−13.

(35) Tao, J.; Guo, A.; Liu, G. J. Adsorption of Polystyrene-Block-Poly(2-Cinnamoylethyl Methacrylate) by Silica from Block-Selective Solvent Mixtures. *Macromolecules* **1996**, *29*, 1618−24.

(36) Tao, J.; Guo, A.; Stewart, S.; Birss, V. I.; Liu, G. J. Polystyrene-Block-Poly(2-Cinnamoylethylmethacrylate) Adsorption in the Buoy-Dominated Regime. *Macromolecules* **1998**, *31*, 172−75.

(37) Tao, J.; Liu, G. J. Polystyrene-Block-Poly(2-Cinnamoylethyl Methacrylate) Tadpole Molecules. *Macromolecules* **1997**, *30*, 2408−11.

(38) Wang, Y.; Li, X. Y.; Hu, H.; Liu, G. J.; Rabnawaz, M. Hydrophilically Patterned Superhydrophobic Cotton Fabrics and Their Use in Ink Printing. *J. Mater. Chem. A* **2014**, *2*, 8094−102.

(39) Dupont *Dupont Krytoxy Performance Lubricant*.

(40) Kim, J.; Efimenko, K.; Genzer, J.; Carbonell, R. G. Surface Properties of Poly[2-(Perfluorooctyl)Ethyl Acrylate] Deposited from Liquid Co2 High-Pressure Free Meniscus Coating. *Macromolecules* **2007**, *40*, 588−97.

(41) Hirao, A.; Sugiyama, K.; Yokoyama, H. Precise Synthesis and Surface Structures of Architectural Per- and Semifluorinated Polymers with Well-Defined Structures. *Prog. Polym. Sci.* **2007**, *32*, 1393−438.

(42) Gao, L. C.; McCarthy, T. J. A Perfectly Hydrophobic Surface (θ_A/θ_R = 180°/180°). *J. Am. Chem. Soc.* **2006**, *128*, 9052−53.

(43) Urata, C.; Masheder, B.; Cheng, D. F.; Hozumi, A. Unusual Dynamic Dewetting Behavior of Smooth Perfluorinated Hybrid Films:

Potential Advantages over Conventional Textured and Liquid-Infused Perfluorinated Surfaces. *Langmuir* **2013**, *29*, 12472−82.
(44) Marchionni, G.; Ajroldi, G.; Cinquina, P.; Tampellini, E.; Pezzin, G. Physical-Properties of Perfluoropolyethers - Dependence on Composition and Molecular-Weight. *Polym. Eng. Sci.* **1990**, *30*, 829−34.